Contrast in Metal−Ligand Effects on Pt_nM Electrocatalysts with M Equal Ru vs Mo and Sn As Exhibited by in Situ XANES and EXAFS Measurements in Methanol

Frances J. Scott,[†] Sanjeev Mukerjee,*[,‡] and David E. Ramaker*[,†]

Department of Chemistry, The George Washington University, Washington, D.C. 20052, and Department of Chemistry, Northeastern University, Boston, Massachusetts 02115

Received: September 4, 2009

In situ X-ray absorption spectroscopy (XAS) measurements, at the Pt L_3 edge (XANES and EXAFS), were carried out on carbon-supported Pt_nMo and PtSn electrocatalysts in an electrochemical cell in 1 M $HClO_4$ with 0.3 M methanol. The CO, OH, and H relative adsorbate coverages on Pt are determined as a function of the applied potential via the ΔXANES technique and compared with comparable data previously reported for Pt_nRu. The more reactive Sn and Mo atoms on the Pt surface form the oxide over the potentials of interest, while Ru has variable oxide content depending on Ru island size and potential. The strength of the electronic ligand effect appears to increase in the order Ru < MoO_n < SnO_n < RuO_n, where the Pt−CO bond strength is found to decrease and the Pt−OH bond strength increase with ligand effect. In the Sn and Mo bimetallics, the ligand effect is found to be sufficiently strong to allow CO replacement by H_2 at low potentials. These widely different ligand effects may provide a straightforward explanation for the previously observed anode behavior in fuel cells: Pt_nMo better in reformate but Pt_nRu better in methanol.

1. Introduction

Improvement in the performance of proton exchange membrane (PEM) fuel cell performance is an area of great interest in the race to produce efficient, economic alternative power sources. Currently, due to H_2 storage and other issues, PEM fuel cells are often more conveniently fed either with reformed H_2 generated at the fuel cell or with liquid fuel such as methanol. Both reformate and methanol introduce CO, the main poison of fuel cells. As little as 10 ppm CO is known to poison Pt catalysts irreversibly.[1] Therefore, the development of more CO-tolerant catalyst materials is crucial to the advancement of fuel cell technology.

One method that has been explored to increase the CO tolerance of catalytic material is to incorporate a second transition metal with the traditional Pt. This method has the added advantage of reducing the amount of costly Pt needed for the catalyst. A variety of Pt−M bimetallic nanocrystals and M-decorated Pt single crystals have been investigated, with the second metal being Ru,[2−31] Mo,[18,19,21,22,32−35] Sn,[17,20,36−48] and other transition metals.[2,49−51] The catalytic enhancement from the addition of the second metal is generally accepted to derive from two mechanisms.[10,15,16,38,52] In the bifunctional (BF) mechanism, water activation,

$$M + H_2O \rightarrow OH/M + e^- + H^+ \quad (1)$$

occurs more readily at the second metal surface, yielding bound OH/M, to which CO can then migrate and be oxidized, as in

$$CO/Pt + OH/Pt \rightarrow Pt + M + CO_2 + e^- + H^+ \quad (2)$$

In the direct electronic, or ligand, mechanism, the second metal acts as a promoter, changing the electronic properties of the Pt such that water activation occurs at lower potentials on Pt, or the Pt−CO bond is weakened, or both. We have previously[53] presented evidence for three distinct potential regions where CO removal by one of the above mechanisms dominates, namely the BF mechanism below 0.25 V (RHE), the direct surface ligand (Dsl) mechanism between 0.25 and 0.5 V, and the direct interior ligand (Dil) mechanism above 0.5 V. The three mechanisms here are distinguished primarily by the source of the OH which oxidizes the CO; either on the Ru islands, next to the RuO(H) islands, or directly on the Pt away from the islands, respectively. We further distinguished between two types of ligand promotion for OH/Pt, which arise as a result of M atoms at the surface and a weaker effect based on M atoms in the interior of the cluster. In that previous work, we found that the particle morphology, as well as the Ru island size, played a large role in determining which mechanism was dominating overall.

One might expect that changing the adatom from Ru to Mo or Sn would significantly change the mechanism in dramatic and even unpredictable ways. Ru is a Pt-group metal sharing common properties with Pt in that it adsorbs both H and CO and has reversible OH adsorption at potentials less than 0.7 V. We and others have noted previously[53] that in PtRu, these properties are synergistic in that the Ru can impart more oxophilic character to the Pt, and vice versa. However, Mo and Sn are very different from Pt. Their surfaces are covered by a tetravalent oxide at potentials above 0.2 V and Pt is known to stabilize both.[35] In this regard, Sn and Mo are similar in that they are dramatically affected by the Pt, with very strong intermetallic bonding.[35] Many[11−14,25,32,54] have noted previously that Ru primarily affects the nearby Pt, but it appears Pt in a "reverse" ligand effect may alter the Sn and Mo islands much more when the M island size is small. Do MoO_x and SnO_x

* To whom correspondence should be addressed. E-mail: s.mukerjee@neu.edu (S.M.); ramaker@gwu.edu (D.E.R.).
[†] The George Washington University.
[‡] Northeastern University.

10.1021/jp908582r
Published on Web 10/22/2009

islands also affect the nearby Pt, and if so how and to what extent? That is a question we consider in this work. We examine the effect of changing the adatom identity by comparing our previous results on three different Pt_nRu electrocatalysts with three new catalysts; two Pt_nMo and a PtSn electrocatalyst. We determine and compare CO, O(H), and H_{upd} (under potential deposited) coverages as a function of potential on the Pt surface utilizing in situ Pt L_3 edge X-ray absorption data with the $\Delta\mu$ analysis technique, as well as the EXAFS analysis technique to gain information on the size and morphologies of the clusters.[53]

2. Experimental Section

Materials. Three types of carbon-supported Pt-based electrocatalysts were used for preparation of the anodes. 30% PtMo (3:1 and 4:1) and 30% PtSn (1:1) were obtained from DeNora N.A. ETEK Division (Somerset, NJ), hereafter referred to as Pt_3Mo, Pt_4Mo, and PtSn, respectively. The anode (working) electrodes were prepared in-house with a metal loading of ~45 mg/cm^2 by a standard vacuum table paper making technique.[36] The metal loading was chosen on the basis of absorption cross sections for Pt and Ru to ensure a step height of close to 1 for the XAS measurements. The electrodes were soaked in 1 M $HClO_4$ for 48 h, followed by vacuum impregnation.

The sealed compression cell used to obtain in situ XAS data has been described in detail elsewhere.[55] The membrane electrode assembly (MEA) was made by sandwiching a Nafion 1135 (1100 MW, 3.5 mm thick) membrane between the prepared anode and a Grafoil (carbon/graphite foil) counter electrode. The electrolyte used in these experiments was 1 M $HClO_4$ with the addition of 0.3 M methanol. The reference electrode was a reversible hydrogen electrode (RHE). These MEAs were prepared by Dr. R. Craig Urian.[56]

X-ray Absorption. An Eco Chemie Autolab PGSTAT-30 potentiostat/galvanostat was used for potential control of the electrodes for XAS experiments. X-ray absorption data were taken at the National Synchrotron Light Source (NSLS) at Brookhaven National Laboratory at beamlines X23A2 and X11A in transmission mode with a three-detector setup.[56] The NSLS storage ring operated at 2.8 GeV and a current between 120 and 350 mA. The three detectors collected incident (I_0), sample (I), and foil transmission data (I_{ref}), i.e., the electrochemical cell was placed between the first and second detector, and a reference foil of the metal of interest was placed between the second and third detectors. The transmission data of the reference foil was used for alignment, as described later. The Si(111) crystal monochromator was detuned by 15% for the Pt edges to exclude higher harmonics. Measurements were taken at the Pt L_3 and L_2 edges at the following potentials in time sequence—PtSn: 0.0, 0.24, 0.40, 0.54, 0.70, and 0.40 V (returning); Pt_nMo: 0.0, 0.24, 0.54, 0.84, and 1.14 V (with respect to RHE)—however, only the L_3 edges were analyzed.

3. Data Analysis

XANES Analysis. Analysis of the XANES (near-edge) region of the XAS data was carried out using the $\Delta\mu$ technique,[57−64] previously applied to adsorption of H, O, and OH on Pt[57] and Pt−M (M = Cr, Fe, Co, and Ni) cathodes[64] and Pt−Ru anodes[53] in an electrochemical cell, and even to Pt and PtRu anodes in an operating direct methanol fuel cell.[65] A brief summary is given here for clarity and to highlight slight differences from the previous method.

The absorption coefficient, μ, was obtained from the raw data using the ATHENA code of Ravel and Newville.[66] After linear combination of appropriate channels of the raw data, the pre-edge background is removed using the AUTOBK algorithm, described more fully elsewhere,[67] followed by normalization over the 20−150 eV (relative to the edge) range for XANES analysis. This procedure was carried out for both the sample data ($\ln I_0/I$) and the reference foil data ($\ln I/I_{ref}$). The foil data were then aligned with each other using a group-developed code, and the resultant energy differences were transferred to the sample data, i.e., the ΔE determined for the foil at x potential is added to the energy of the data at the same x potential. This energy calibration corrects for shifts due to photon beam drift and other possible effects. This energy calibration is crucial for the success of the $\Delta\mu$ technique to ensure full cancellation of the atomic contribution in the XANES, which dominates the spectrum, i.e., $\Delta\mu$ is typically only about 1−5% of the total μ signal.

The difference $\Delta\mu = \mu(V) - \mu(V_{ref})$ is generally determined by subtracting the μ at an appropriate reference potential, V_{ref}, (usually taken to be that potential at which the electrode is relatively free of most adsorbates) from other potentials to highlight the effect of these adsorbates. However, the choice of reference can change on the basis of the sample, the adsorption edge, and the operating conditions. In this work, 0.54 V in 1 M $HClO_4$ without methanol was used as the reference to determine CO and H_{upd} coverages for the Pt_nMo samples. However, in the case of the PtSn, the samples in and out of methanol were not comparable, and therefore, 0.40 V on the return in methanol was used as reference, as in our previous work with Pt_nRu catalysts.[53] This potential has been determined to contain the least amount of CO, as most of the CO has been oxidized off and only a comparably smaller amount readsorbed, and neither H or O(H) are heavily adsorbed in this potential region. Therefore, the CO signal, as well as the H_{upd} signal, can be obtained from the difference,

$$\Delta\mu(x, \mathrm{CO, H}) = \mu(x, \mathrm{Me}) - \mu(0.40R, \mathrm{Me}) \quad (3a)$$

for PtSn and

$$\Delta\mu(x, \mathrm{CO, H}) = \mu(x, \mathrm{Me}) - \mu(0.54) \quad (3b)$$

for Pt_nMo. As will be shown in Figure 2, CO and H_{upd} (i.e., under potential deposited H in a 3-fold site[68]) were visible as two distinct features by this method, allowing for simultaneous determination of their coverages.

Because CO and O(H) have been shown to coadsorb[53] and because their signals contain areas of overlap, a more complex method was used to extract the O(H) (i.e., O or OH) signal. In this case, 0.24 (Pt_3Mo, PtSn) or 0.54 V (Pt_4Mo) in methanol is used as the reference. At both these potentials, neither H nor O(H) should be contributing significantly to the signal. As the reference in this case does contain contributions from CO, it is necessary to add a scaled portion of the CO signal $\Delta\mu(0.24, \mathrm{CO})$ from eq 3a back in, to remove this CO contribution to the signal. The scale factor, a, is chosen to minimize $\Delta\mu$ in the positive CO region (~7.5−11 eV relative to the Pt edge). Thus,

$$\Delta\mu(x, \mathrm{O}) = \mu(x, \mathrm{Me}) - \mu(0.24\ \mathrm{V, Me}) + a\Delta\mu(0.24\ \mathrm{V, CO}) \quad (4a)$$

for Pt_3Mo and PtSn and

$$\Delta\mu(x, \mathrm{O}) = \mu(x, \mathrm{Me}) - \mu(0.54\ \mathrm{V}, \mathrm{Me}) + a\Delta\mu(0.54\ \mathrm{V}, \mathrm{CO}) \quad (4b)$$

for Pt_4Mo.

EXAFS Analysis. EXAFS analysis was carried out using the ATHENA and ARTEMIS codes.[66] The absorption coefficient, μ, was obtained from the ATHENA program in a manner identical to that described above for the XANES region, with the exception that the normalization range was changed to 150 to ~1600 eV relative to the edge. A FEFF 8.0[69] calculation on a Pt_4M_2 "Janin cluster"[70] (Figure 1) was imported to model the Pt−Pt and Pt−Ru paths at the platinum edge. The many-body S_0^2 calculated by FEFF 8.0 was 0.934 for the platinum edge. ARTEMIS calculates a factor called amp for each path that corresponds to S_0^2, and the degeneracy of the path in the model we indicate by N(model). Because S_0^2(FEFF8)/N(model) ≅ amp/N(fit)

$$N(\mathrm{fit}) = \mathrm{amp}*N(\mathrm{model})/S_0^2(\mathrm{FEFF}) \quad (5)$$

FEFF 8.0 Calculations. The FEFF 8.0 code[69] was also used to model the adsorbate $\Delta\mu$ signatures. The $\Delta\mu$(Ads) was determined by subtracting the μ of a clean "Janin-type Pt_4M_2 cluster"[70] from the μ of a cluster containing an adsorbate molecule in the atop, bridged, or n-fold position (Figure 1), i.e., $\Delta\mu = \mu(\mathrm{O/Pt_4M_2}) - \mu(\mathrm{Pt_4M_2})$. The "Janin cluster", used in much but not all of our previous work,[57−64] was chosen here because it is about the smallest cluster that contains atop, bridged, fcc, and hcp sites. The bond distances used in the clusters were the same as those in our previous FEFF 8.0 calculations.[53] Oxygen in the atop position was treated as OH (since the scattering from H is negligible), while oxygen in an n-fold position was treated as O. This is consistent with chemical intuition and density functional theory (DFT) calculations,[57] which show that OH prefers to be singly coordinated, and O doubly or triply. In FEFF 8.0, a unique potential was calculated for each Pt, M, and adsorbate atom to allow for different surroundings of each atom.

4. Results

XANES Analysis. Figure 2a shows typical Pt L_3 edge $\Delta\mu$ spectra emphasizing the CO and H fcc (H_{upd}) signals, compared with the theoretical atop signal for CO and the fcc signal for H, calculated using FEFF 8.0. The magnitude of each peak (negative for H_{upd} and positive for CO) in the highlighted region was evaluated to determine the relative amounts of H and CO present at different potentials. The heights are then divided by the heights of the comparable theoretical signals, in order to estimate coverage, as will be described more fully later.

Figure 2b shows representative Pt L_3 edge $\Delta\mu$ spectra, in this case emphasizing the contribution of oxygen to the spectra, which was partially hidden (although evident as negative features) in Figure 2a by the negative portion of the CO peak in the −2 to 7 eV range. As seen previously,[53] three peaks are visible in the oxygen region, corresponding to (in increasing energy) OH atop "near" an M island, OH atop "away from" an M island, and O in an n-fold position (referred to in this work as OH_{near}, OH_{away}, and O). Due to the small size of the "Janin cluster" (Figure 1), it is not expected that a differentiation can be made between OH_{near} and OH_{away} in a FEFF 8.0 calculation on a small Pt_4M_2 cluster, as necessarily all atoms are "close" to each other. However, we can mimic the effect of OH_{away} by modeling O(H) on a simple Pt_6 Janin cluster (i.e., without any M atoms present). Although a single FEFF 8.0 calculation does not reproduce the three peak structure seen in the data, nor reproduce the full shift, FEFF 8.0 does predict twice the gap in energy between the atop and n-fold positions in the Pt_4M_2 cluster compared to the Pt_6 cluster. Figure 2b shows the FEFF 8.0 calculated individual $\Delta\mu$ signals in which the OH_{near} result has been moved down to mimic the doubled energy gap between the atop and n-fold positions.

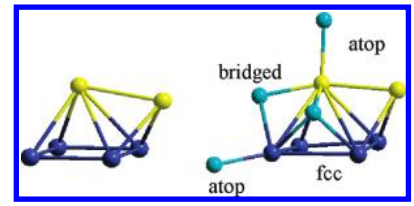

Figure 1. Representative clean Pt_4M_2 Janin cluster and with adsorbate in atop, bridged, and fcc positions.

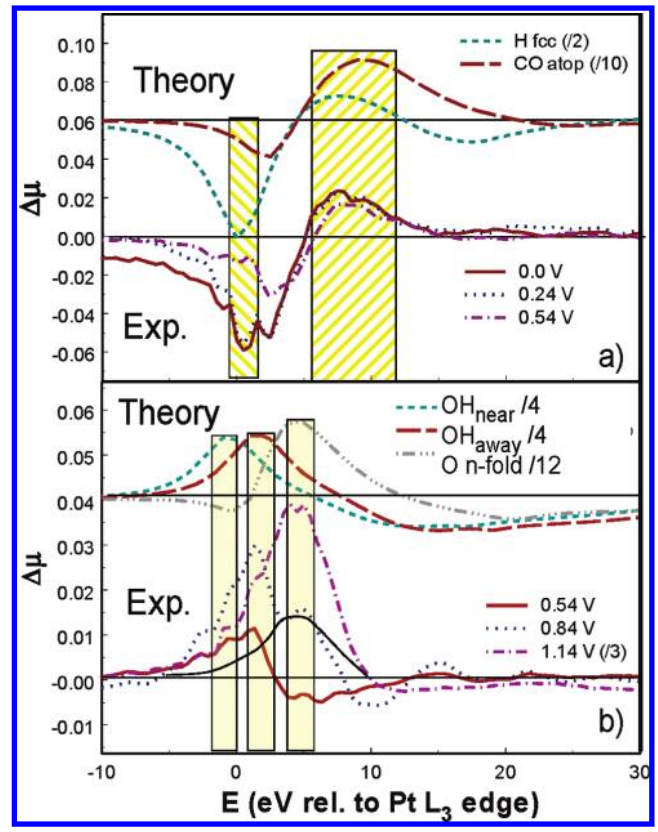

Figure 2. (a) Pt L_3 edge $\Delta\mu$ spectra for Pt_4Mo using eq 3a and compared with theoretical signatures from FEFF 8.0 for CO adsorbed in an atop site and for fcc H. (b) Pt L_3 edge $\Delta\mu$ spectra for Pt_3Mo using eq 4a and comparison with theoretical signatures for atop OH and n-fold O. The shaded areas in (a) and (b) indicate regions utilized to determine relative coverages with corrections as discussed in text.

The relative shift in the energy positions of OH_{near} and OH_{away} has been seen before in bimetallics when some M (M = Cr, Fe, Co, Ni, and Ru) atoms are at the surface, but not when they are absent.[64,65] This shift is believed to arise in part from a Pt L_3 core level shift occurring as a result of charge transfer between the M and nearby Pt atom (i.e., a ligand effect). Further, XANES analysis of pure Pt samples does not show the lowest energy OH_{near} peak, giving further evidence that this peak is the result of the mixed metal morphology.[57] The height of each experimental $\Delta\mu$ peak in the indicated highlighted regions was used to determine the relative coverage of O(H) species at each potential.

Figure 3 shows the relative coverage change for each indicated adsorbate species determined from the $\Delta\mu$ amplitudes

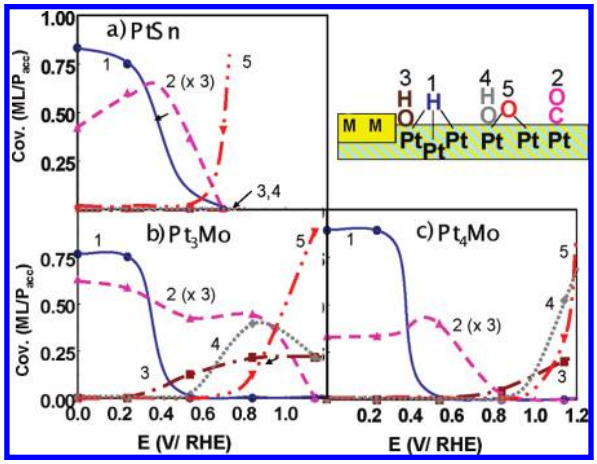

Figure 3. ML adsorbate/Pt_{acc} for the various adsorbates on the indicated catalysts obtained by scaling $\Delta\mu$ XANES amplitudes by the appropriate scale factors as described in text.

in the shaded regions, as shown in Figure 2 and similar plots of $\Delta\mu$ for the other catalyst but scaled by factors as discussed below to yield coverages in monolayers (ML) per accessible Pt atom. To arrive at these results, corrections were included to allow for overlap of the coadsorbate signatures. For example Figure 2a shows that a significant contribution from $\Delta\mu(H_{upd})$ will appear in the experimental $\Delta\mu$ at 10 eV, where the magnitude for estimating the CO coverage is made. This overlap between $\Delta\mu(H_{upd})$ and $\Delta\mu(CO)$ is accounted for by subtracting out the $\Delta\mu(H_{upd})$ contribution before estimating the CO coverage; the $\Delta\mu(H_{upd})$ magnitude determined at 0 eV, where the $\Delta\mu(CO)$ is nearly negligible, and the $\Delta\mu(H_{upd})$ line shape determined from the theory. Much stronger overlap exists between the 3 different O(H) signatures in Figure 2b, particularly at high potential (above 0.8 V) when the $\Delta\mu(O_{n\text{-fold}})$ dominates and the $\Delta\mu(OH_{away})$ introduces just a small feature on top of this larger one. Resolution of these three contributions might possibly be improved by fitting two or three Gaussian-type functions to the experimental $\Delta\mu$, but this was not attempted in this work.

Figure 3 shows that H_{upd} in the fcc sites is present at 0.0 V, and at slightly lower coverage at 0.24 V, before being oxidized off by around 0.35 V. CO is also present at low potentials reaching a significant level in most cases around 0.5 V, when the H_{upd} and OH coverages are at a minimum. In general, the CO coverage decreases as the OH coverage increases, reflecting the reaction between adsorbed CO and OH (i.e., via either the bifunctional or ligand mechanism). Differences between the onset for OH_{near} will be discussed below.

EXAFS Analysis. The EXAFS analyses of the three electrocatalysts at the Pt L_3 edge are summarized in Table 1. In all cases, the Debye−Waller factor, σ^2, was held at 0.005 Å^2, exactly as done previously for the Pt_nRu catalysts[53] to allow meaningful comparison of N for all cases. The magnitudes of N_{Total} at the platinum edge indicate particle sizes ranging from about 1.3 to 2.3 nm, on the basis of model cluster calculations assuming spherical clusters.[71,72] Although it is not claimed that these are perfectly spherical clusters, this does illustrate the difference in size (1.3−2.3 nm) and dispersion (0.56−0.90) of the catalysts.

Converting $\Delta\mu$ Magnitudes to Absolute Coverage. The magnitudes of the various $\Delta\mu$ features of interest were measured, as indicated in Figure 2. These magnitudes were then divided by the absolute height of the relevant FEFF 8.0 calculation, shown also in Figure 2. Since the Janin cluster (Figure 1) used for the FEFF 8.0 calculations has a Pt−Ad coordination number of 1 (i.e., the photon absorber Pt atom is always placed next to the adsorbate (Ad)), after applying these scale factors S_{ad} (i.e., $\Delta\theta_{ad} = S_{ad}M_{\Delta\mu}$),[73] one obtains a reasonable measure of the coverage change from the reference (i.e., $\Delta\theta_{ad}$) in units of ML adsorbate per total absorber atom (M_{tot}, where 1 indicates one adsorber atom for each Pt atom). This coverage change is relative to M_{tot} because the XAS spectra are normalized to one and the XAS samples all atoms present in the beam cross-sectional area. Using this method, we obtain at 0.0 V RHE, CO coverages for PtSn, Pt_3Mo, and Pt_4Mo, of approximately 0.025, 0.06, and 0.05 ML/M_{tot}, respectively, and H_{upd} coverages of 0.14, 0.17, and 0.37 ML/M_{tot}, respectively. As discussed previously, these estimates are only semiquantitatively correct because the conversion factors may vary with coverage (e.g., each surface CO in an fcc binding site is coordinated to three Pt atoms, while at a different coverage the CO may prefer a corner/edge atop site, which is coordinated to just one Pt atom).[68] Further, the FEFF8 $\Delta\mu$ amplitudes, although normally quite reliable, are particularly suspect for the very light H atom where the single 1s orbital can become highly distorted by bonding with the Pt, and hence not be reproduced accurately by the muffin-tin calculations done in FEFF8. Nevertheless, we have previously calibrated the $\Delta\mu$ scale factors for H using gas-phase H_2 chemisorption results at different temperatures and pressuress to determine the absolute H coverages,[74] and found the coverages estimated from $\Delta\mu$ amplitudes to be quite reliable. Thus the estimated adsorbate coverages are semiquantitatively correct, and these can be very helpful in understanding the relative activity of the different CO oxidation mechanisms. Further, estimating coverages on these samples makes possible comparison with the previous Pt_nRu samples.

Although these magnitudes represent actual change in coverage ($\Delta\theta_{ad}$) from the reference potential, they essentially indicate absolute coverage (θ_{ad}) for all but the CO/PtSn case. Recall, for the determination of CO and H fcc on Pt_nMo, the μ at 0.54 V in 1.0 M $HClO_4$ with no methanol was used as the reference. CO should not be present in the reference, as no methanol is present, and fcc H is known to be removed from the surface by 0.54 V. The reference used for O(H) determination was either 0.24 or 0.54 V, where no O(H) is found or believed to be present on the relevant samples either. The only reference, therefore, which contains an adsorbate species of interest is 0.40 V on the return, used to determine CO coverage on PtSn. Rough estimates of the CO coverage on PtSn at 0.40 V on the return can be obtained from the $\Delta\mu$ signals. Although, as mentioned above, the samples in solution without methanol were not found to be directly comparable to those in methanol for the PtSn case (i.e., the Pt clusters appeared to experience shape or morphological changes so that the large Pt−Pt EXAFS contributions did not cancel completely upon taking the difference), they were similar enough to allow for some comparison of the CO coverages. Using the 0.54 V 'clean' (i.e., no methanol) spectrum as a reference, the ratio $[\theta_{CO/Pt}(0.24\text{ V}) - \text{clean}]/[\theta_{CO/Pt}(0.24\text{ V}) - \theta_{CO/Pt}(0.4R)]$ determined from the relative size of the $\Delta\mu$ amplitudes was found to be 3 ± 0.3. Assuming full coverage at 0.24 V is 0.20 ML (see below), means $0.20/(0.20 - \theta(0.4R)) = 3$, or $\theta(0.4R) = 0.13$; that is, ~2/3 of the maximum coverage is still present at 0.40 V on the return.

Catalysts Utilization. In our previous work with the Pt_nRu catalysts,[53] it was shown that the number of electrochemically accessible Pt absorber atoms (Pt_{acc}), and thus their coverage by adsorbate, could be related to the total number of Pt atoms (Pt_{tot}), by accounting for several factors, including the dispersion *D*

TABLE 1: Summary of in Situ EXAFS Results from Pt L_3 Edge at 0.54 V RHE (Pt_nMo) and 0.58 V RHE (PtSn) in 1 M $HClO_4$

catalyst	N_{Pt-Pt}[a]	R_{Pt-Pt} (Å) ± 0.02	σ^2 (Å^2)	E_0 (eV) ± 1 eV	N_{Pt-M}[a]	R_{Pt-M} (Å) ± 0.02	σ^2 (Å^2)	E_0 (eV) ± 1 eV	N_{Total}[a]	N_{Pt-M}/N_{Pt-Pt}
PtSn	6.3	2.79	0.005	−0.678	1.4	2.76	0.005	−0.504	7.7	0.2
Pt_3Mo	5.9	2.76	0.005	1.588	1.7	2.76	0.005	5.535	7.6	0.3
Pt_4Mo	7.9	2.77	0.005	1.303	1.4	2.77	0.005	3.595	9.3	0.2

[a] Although the absolute errors are of the order of 20%, the changes with catalysts are expected to be meaningful to 0.1 because of the fixed σ^2.

TABLE 2: Comparison of Various Properties of the Six Electrocatalysts Considered

property	PtRuW	Pt_3Mo	PtSn	Pt_3RuW	PtRuE	Pt_4Mo
N_{total}	7.2	7.6	7.7	8.3	8.6	9.4
diameter[a] (nm)	1.3	1.4	1.4	1.6	1.7	2.3
dispersion[b]	0.90	0.83	0.82	0.74	0.7	0.56
nN_{PtRu}/N_{PtPt}[c]	0.64	0.87	0.22	0.30	0.42	0.71
thres(O_{br}/Pt)[d]	0.3 (0.5)	0.6	0.6	0.4	0.7	0.8
$DF_{cont}F_{cov}$[e]	0.19	0.22	0.17	0.27	0.19	0.42
$F_{cont}F_{cov}$[e]	0.21	0.27	0.21	0.36	0.27	0.75

[a] Calculated assuming spherical particles[71,71] with uncertainty = ±0.2. In general EXAFS gives particles sizes about 50% smaller than that from XRD or TEM. N_{PtPt} from Table 1 and similar results for Pt_nRu reported elsewhere.[53] [b] Based on particle diameters indicated.[71] [c] n = Pt/M molar ratio and N_{PtRu} and N_{PtPt} from Table 1 and similar results for Pt_nRu. Relative uncertainty = 40%. [d] Threshold potential (V, RHE) for O_{br}/Pt from Figure 2 and similar results for Pt_nRu reported elsewhere.[53] Uncertainty = ±0.1 V. [e] See text.

(fraction of Pt atoms at the surface of a cluster), cluster contact (F_{cont} = fraction of surface Pt atoms still accessible after support and neighboring cluster contact), and F_{cov} = fraction of surface atoms not covered by M islands on the surface; that is,

$$Pt_{acc} = Pt_{tot}DF_{cont}F_{cov} \quad (6)$$

Here Pt_{acc}/Pt_{tot} is related to the electrochemical surface area (ECSA) typically reported in m^2 Pt/gPt, but now as a unitless number representing fractional loss.

We can estimate the fractional loss by making a few assumptions. It has been previously shown that the maximum coverage for CO on Pt(111) in a (2 × 2)-3 CO unit cell is about 0.75 ML.[75] However, in the current work H_{upd} comes on the surface at low potentials (this was not seen with PtRu), so that the CO coverage does not reach a full 0.75 ML at low potentials. Therefore, we will assume here that the H_{upd} + CO coverage at low potentials reaches 1 ML/Pt_{acc}, so that

$$(\text{ML ads}/Pt_{acc})/(ML_{from\Delta\mu}/Pt_{tot}) = 1/[\theta_H+\theta_{CO}]_{from\Delta\mu} = Pt_{tot}/Pt_{acc}$$

This gives us the ratio Pt_{tot}/Pt_{acc} that relates directly to $DF_{cont}F_{cov}$, as tabulated in Table 2.

The total OH + O coverage at 1 V is also around 1 ML/Pt_{acc}, as expected, confirming that the conversion factors utilized above for CO + H_2 are also reasonable for OH + O. We note again that although the final estimated adsorbate coverages, θ(ML)/Pt_{acc}, represent reasonable estimates of the coverage in situ on real supported Pt catalysts, they are still only slightly better than qualitative for the reasons discussed above, but even such estimates are difficult to obtain by other means.

Table 2 also gives a summary of the total Pt EXAFS coordination, $N_{total} = N_{PtPt} + N_{PtM}$, for the three Pt_nM catalysts in this work and the three Pt_nRu catalysts considered previously.

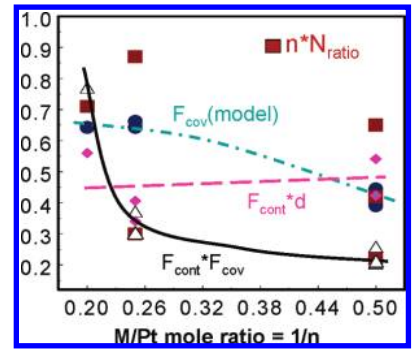

Figure 4. Plot of several parameters from Table 2 as discussed in the text with the M/Pt mole ratio.

The estimated diameter assuming spherical particles and these N_{tot} values are given along with the dispersion (fraction of atoms at the surface).[71,72] Having the estimated dispersion we can estimate $F_{cont}F_{cov}$, which is tabulated in Table 2 and plotted in Figure 4 along with the ratio nN_{PtRu}/N_{PtPt} as a function of n, the Pt/M molar ratio.

Figure 4 clearly shows that $F_{cont}F_{cov}$ decreases sharply with the M/Pt mole ratio, but a large scatter exist with nN_{PtM}/N_{PtPt}, a factor that one might expect would reflect the morphology of the cluster. The continuous decrease in $F_{cont}F_{cov}$ with M/Pt suggests that the M atoms exist primarily at the surface of the Pt core, and as M/Pt increases more of the Pt sites are covered by the M atoms. Further, the absence of a correlation between $F_{cont}F_{cov}$ and nN_{PtM}/N_{PtPt} suggest that the latter does not in fact indicate the morphology of the cluster (i.e., the distribution of M in the cluster), but rather the oxidation level of the M atoms on the surface, since oxidiation of the surface islands, including insertion of O between Pt and M atoms, will decrease the Pt−M coordination. In our previous work we indeed showed from the Ru K edge EXAFS data that the Pt_3RuE and Pt_3RuW clusters had a significant fraction of oxidized Ru on their surfaces, and the PtRuW islands were smaller and less oxidized, consistent with the relative sizes of nN_{PtM}/N_{PtPt} in Table 2. Further nN_{PtM}/N_{PtPt} is quite small (0.2) for PtSn, consistent with the Sn at the surface being heavily oxidized. The much larger values for Pt_nMo (0.7−0.9) seem to suggest that the Mo islands are not heavily oxidized above 0.2 V, but we will provide arguments below (Figure 11) that they are. The larger nN_{PtMo}/N_{PtPt} values may just hint at the stronger interaction between Pt and Mo, so that O cannot insert itself between the atoms of the Pt core and MoO_x islands so easily, with the oxide layer more on the outer surface in contrast to that for Ru and Sn that have a weaker interaction with Pt. However, this is only conjecture.

Assuming most of the M atoms are on the Pt surface core, one can then estimate F_{cov} (fraction of surface atoms not covered by M islands) with the simple expression, $F_{cov} = 1-1/[(n+1)D] = 1 - n_M/n_{Surf}$, where n_M/n_{Surf} indicates the simple ratio of M atoms to total particle surface atoms; this is plotted in Figure 4 along with the resultant estimates of dF_{cont} that appear to be relatively nonvariant at 0.5, where d is the average

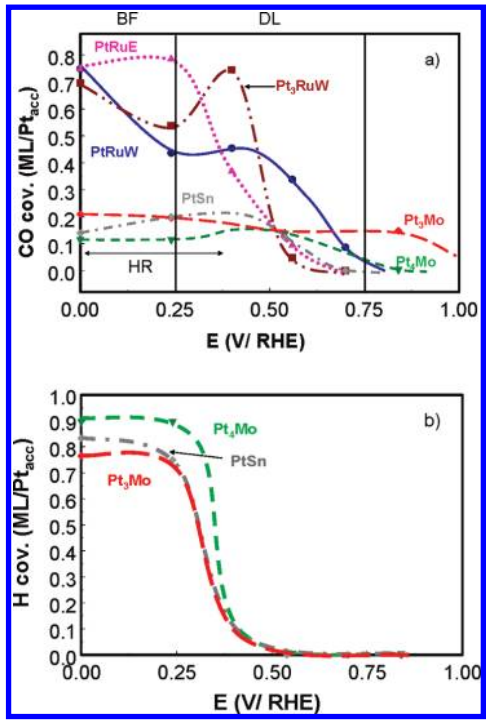

Figure 5. (a) CO coverage and (b) H_{upd} coverage in units of ML/Pt_{acc}, with the potential regions of activity for different CO oxidation mechanisms indicated. No H_{upd} was seen for the PtRu catalysts.

estimated particle diameter indicted in Table 2. Figure 4 shows that F_{cont} (fraction of surface Pt atoms still accessible after support and neighboring cluster contact) various roughly as 0.4d until it reaches 1.0, i.e., small particles suffer a large contact reduction as expected, and this factor goes to 1 as the particle size goes above 2.5 nm.

The estimate above that only one out of every three or four surface Pt atoms is actually electrochemically accessible for catalysis/adsorption on particles less than 1 nm is not surprising considering the relatively high loading utilized here for XAS analysis. Wang et al.[76] suggested a contact factor of 0.7 for much larger 13-nm particles and much lower loading than in this work (both factors should increase F_{cont}). Earlier electrochemical and microscopy catalysts utilization studies indicated that much of the Pt might be inaccessible due to particle agglomeration and other ionic/electronic isolation mechanisms, and found it to depend on the Pt/Nafion ratios, composition, processing techniques, electrolyte, etc.[77−81] as one might expect. The ECSA in m^2 Pt/g Pt can easily change by a factor of 2 or more even for 20 wt % E-tek Pt/VC (Vulcan carbon) electrodes (i.e., without a second M) just by varying the electrolyte.[77]

Effect of the Metal M on the Dominant Mechanism. Figure 5a compares the estimated CO/Pt coverages ($\Delta\theta$ in ML/Pt_{acc}) for PtSn, Pt_3Mo, and Pt_4Mo, as well as for the three Pt_nRu samples previously examined. This figure also indicates the effective experimental ranges previously determined for each of the CO oxidation mechanisms;[53] i.e., the BF mechanism is dominant from 0 to 0.25 V, and the direct ligand (DL) effect is dominant from around 0.25 to 0.75 V. As CO is oxidized by OH above 0.7 V on pure Pt, any decrease in CO coverage above this potential is presumed to be independent of the second alloying metal. Figure 5b provides a similar comparison for fcc H_{upd}, Figure 6 for OH_{near} and OH_{away} and Figure 7 for n-fold O.

One can condense all of this data, and better understand it, by estimating the threshold potential for each adsorbate (i.e., for O, OH_{away}, and OH_{near}), as well as the threshold potential

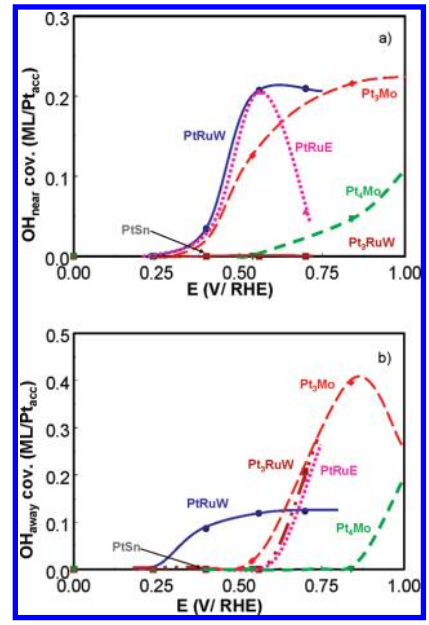

Figure 6. (a) Atop OH_{near} and (b) OH_{away} in ML/Pt_{acc}.

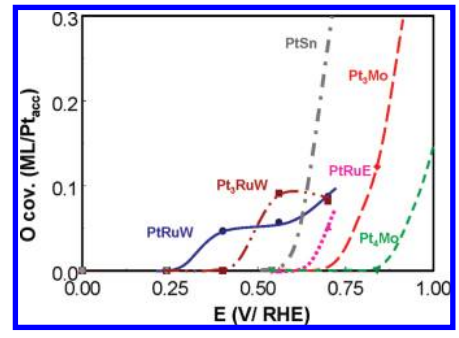

Figure 7. n-fold O coverage on Pt in ML/Pt_{acc}.

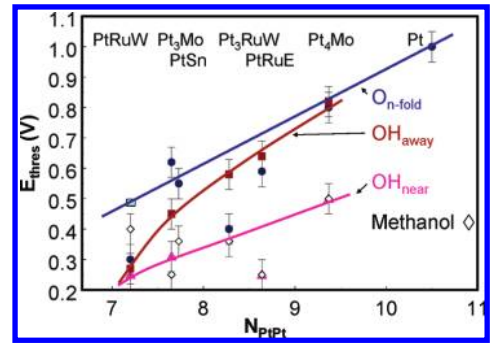

Figure 8. Plot of the estimated OH_{near}, OH_{far}, and n-fold O adsorption thresholds vs N_{PtPt} (the Pt−Pt coordination from the EXAFS data in Table 1) and obtained from the data in Figures 5−7. The estimated thresholds for CO reduction from Figure 4 are also indicated by the open squares. Data point for n-fold O at N_{PtPt} = 10.5 obtained from ref 82.

for CO oxidiation. This is shown in Figure 8 as a function of N_{PtPt}, which reflects the Pt particle sizes. Also included in Figure 8 is a result reported elsewhere[82] for catalysts with large pure Pt particles. Error bars give the estimated uncertainty in these threshold estimates, which are somewhat large because of the paucity of data points.

Figure 8 shows the systematic increase in the adsorbate threshold values with particle size. Note the merging of the threshold for OH and O with particle size, completely consistent with the known near absence of OH on SC Pt(111), and recent theoretical calculations showing the OH and O thresholds

essentially the same for Pt(111).[83] Note that for PtRuW, having the smallest average particle size, the O threshold falls off of the linear trend line. However, the data in Figure 7 reveal two thresholds, which we believe arises from O adsorption near (lower) and removed (higher) from the Ru islands, and the higher threshold (indicated by the blue shaded square in Figure 8) clearly falls on the trend line. The data for Pt_3RuW in Figure 8 do not actually reveal a second threshold, but the nature of the curve suggests that one would also exist in this case if the data were extended, and clearly the first threshold is reflecting a ligand effect from the Ru. Finally, note the gradual loss of the M atom ligand effect on Pt with particle size, as expected, and the unexpectedly large ligand effect for the PtRuE catalyst.

These comparisons reveal some interesting observations:

(a) The agreement in Figure 8, to within experimental uncertainty, between the CO oxidation and OH_{near} adsorption thresholds clearly establishes the direct ligand mechanism as dominant between 0.25 and 0.75 V, and this ligand effect is strongly dependent on particle size.

(b) The most striking difference in the CO coverage between the six catalysts is the large CO coverage on the Pt_nRu catalysts and the dramatically lower CO coverage below 0.3 V for the Pt_nMo and PtSn catalysts. We attribute this to a hydrogen replacement (HR) mechanism, whereby the CO−Pt bond is sufficiently weakened by the M atom ligand effect enabling H_{upd} to replace CO at low potentials. In our previous work, H_{upd} was not seen on the PtRu samples in methanol, suggesting that H_{upd} was unable to displace CO for the Pt_nRu catalysts. We have previously seen[68] where hydrogen replaces CO at low currents (potentials) in reformate for some Pt_nRu catalysts, so that the Ru ligand effect does weaken the CO bond sufficiently to allow some H replacement of the CO in the presence of H_2 gas and weak concentrations of CO; however, apparently not enough to allow this to occur in methanol.

(c) We have noted previously that the BF mechanism is active in the Pt_nRu catalysts when the Ru islands are relatively small. When the islands are small, a reverse ligand effect by the Pt keeps the Ru islands from being fully oxidized, enabling OH adsorption on the Ru (i.e., for the two Pt_nRuW catalysts). In the Pt_nRuE catalysts the islands are bigger and more oxidized, making the BF mechanism inactive but exerting a very strong ligand effect at 0.5 V. Sn and Mo are expected to be more reactive to oxygen than Ru making the BF mechanism inactive in these cases regardless of island size; but this is not important because the HR mechanism below 0.3 is active anyway.

(d) Figure 8 shows that the OH_{near} and O thresholds for PtRuE do not fall on the trend lines but are much lower. We have previously observed the strong ligand effect exhibited by the oxidized Ru islands for this PtRuE catalyst (point c above) and will discuss this further below.

(e) All catalysts have essentially zero CO coverage beyond 0.75 V except for Pt_3Mo; it apparently requires some OH adsorption directly on the Pt (i.e., the OH must come to the CO, rather then the CO coming to the OH on or near the MoO_x islands). The fraction of CO able to migrate to the M islands will be determined by both the density of M islands (presumably inversely proportional to n, the Pt/M ratio) and perhaps cluster size. Cluster size enters because only the CO on the Pt(111) faces is expected to be mobile (as opposed to those on the corner/edges), and the fraction of Pt atoms on the faces increases as the cluster size increases. The Pt_3Mo catalyst has a large n and relatively small particles both consistent with the low fraction of CO able to migrate to the M islands.

TABLE 3: Summary of Previously Reported Pt, PtRu, PtMo, and PtSn Electrocatalysts Properties

characteristic	Pt	Pt_nRu	Pt_nMo	Pt_nSn
rel. CO tol. in H_2,CO[18,19a]	1	1.3	4	1.2
rel. eff. in methanol j @0.4 V[18b]	1	∼5	1	1
CO/M[18,19]	yes	yes	no	no
E_a (Pt−CO), kJ/mol[20,21]	17	17, 4.5	12	3.5
CO react. order[20]	−0.39	−0.46		−0.88
CO ox pot. (V @ thr and pk, 85 °C)[20,19]	0.4	0.22	<0.18	0.18
H_2/100 ppm CO	0.52	0.38	0.39	0.48
CO binding sites[41]	CO_{low}	CO_{low}		CO_{hi}, CO_{low}
CO ox. pot. (V) H_2/.1%CO[35]	0.6	0.35	<0.1, 0.5	
CO ox. pot. (V) sat. CO[41]	0.85	0.60		0.3

[a] CO tolerance based on limiting current at steady state anode polarization in a 5 cm^2 PEMFC under 100 ppm CO in H_2 at 85 °C. [b] Based on limiting current for methanol oxidation at 90 °C with 1 M MeOH and Nafion 117 membrane.

5. Discussion

Performance in Reformate versus Methanol. The results reported above suggest that the Mo and Sn islands are oxidized at all relevant potentials and exert a strong ligand effect on the Pt, while the Ru ligand effect is strongly dependent on the island size, large for the big Ru islands and smaller for the smaller ones. The ligand effects exhibited by Sn, Mo, and Ru for both hydrogen oxidation (HOR) in reformate, and methanol and CO oxidation have been extensively studied previously, so we compare the current results with those found in the literature.

The literature results are summarized in Table 3. These results generally show that Pt_nMo (and perhaps Pt_nSn) catalysts are more effective fuel cell catalysts in reformate than Pt_nRu; however, Pt_nRu is more effective in a direct methanol fuel cell. This difference has been attributed to a number of factors, some noted in Table 3. We discuss these factors in light of the three different mechanisms for CO oxidation listed above, namely the BF, DL, and HR mechanisms. For example, Mukerjee's group (as well as others) have noted that CO can compete for adsorption with OH on Ru, but not on Mo or Sn, similar to that suggested above, ruling out the BF mechanisms for Pt_nMo and PtSn.[18,19]

A second difference between the PtM catalysts has consistently been noted when studying CO oxidation, and that is the difference in the nature of the CO participating in the reaction. Wang et al.[41] have noted that two types of CO exist on PtSn, a "high coverage" CO and a "low coverage" CO, the former bonded much weaker to the surface, and arising only from direct adsorption of CO, (i.e., it cannot be formed from methanol oxidation because methanol requires more than one site to oxidize, and neighboring multiple sites do not exist when the "low coverage" CO already poisons the Pt for methanol oxidation). Therefore, Wang et al. attribute the strong enhancement (factor of 1000) for CO stripping currents in PtSn to oxidation of this "high coverage" CO, which apparently only exists on PtSn during CO exposure.[41] It is probable that the CO_{hi} and its contribution to the oxidation stripping current does not relate directly to the effectiveness of PtSn in reformate and methanol, because the CO_{low} will primarily determine this. We suggest that the CO_{hi} is linearly bonded CO, and CO_{low} is bridged (or even 3-fold) bonded CO. CO is believed to bond in atop sites, and then at higher coverage, because of lateral interactions, some CO is pushed into bridge (and n-fold) bonded sites. SFG studies suggest that CO may even be lying nearly flat at lower coverage.[84] The bridged/linear binding ratio is

highly dependent on coverage, particle size, and even Pt particle support (i.e., acidic or basic).[85] The different order in CO for PtSn observed by Mukerjee et al. (Table 3) may arise from this different CO binding site.

Mukerjee's group has also measured the activation energy for releasing CO from Pt sites during the HOR as summarized in Table 3.[20,21] Because E_a is related to the removal of CO to create active sites for the HOR, it in some sense reflects the nature of the Pt−CO bond strength. These results suggest then that the Pt−CO bond on PtSn and Pt_nMo has a much weaker Pt−CO bond strength compared to that on Pt and PtRu; however, at lower temperature, when the CO coverage is higher, a weaker bonded CO participates also on PtRu. All of these results suggest that the adatom islands weaken the Pt−CO bond in the order, $Ru_1 < Mo < Sn \approx Ru_2$. Here the second E_a for PtRu is interpreted as arising from two different Ru environments (Ru_1 vs Ru_2) rather than two different CO binding sites on Pt (e.g., linear vs bridged as suggested by Lee et al.[21]). As we suggested previously, Ru can exert two widely different or varying ligand effects, depending on the oxidation state of the RuO_x islands, the later determined in part by the Ru island size. Therefore, we suggest that the ligand effect weakening the Pt−CO bonding increases in the order $Ru < MoO_x \approx SnO_x < RuO_x$.

Comparison of the threshold potentials for CO oxidation in reformate (Table 3) indeed suggests that they are all in the range of 20−48 mV consistent with the DL mechanism and Figure 8, but in general they are slightly lower for Mo and Sn than for Ru, suggesting a ligand effect in the order $Ru < SnO_x \approx MoO_x$. Combining these results with those in this work, where we find a very strong ligand effect for RuO_x, we find the methanol oxidation and HOR in reformate results suggest similar trends; namely that the ligand effect increases in the order $Ru < MoO_x \approx SnO_x < RuO_x$.

The results above suggest that the ligand effect weakens the Pt−CO bond, that MoO_x and SnO_x exert a particularly strong ligand effect compared to Ru, and this is most directly confirmed in Figure 5 by the different coverages of CO in methanol. Previously reported[18,86] results summarized in Figure 9 directly confirm this difference between PtRu vs PtMo catalysts also in CO stripping. Here CV curves for Pt are compared with the PtRuE and Pt_3Mo catalyst after dosing with CO at 0.0 V for 1 h, and for Pt_3Mo without exposure to CO (only N_2 for 1 h). Comparison of the two CV curves for Pt_3Mo in the H_{upd} region below 0.3 V does show some CO poisoning, but not near as much as for the Pt and PtRu catalysts. The bottom part of Figure 9 shows the CO electro-oxidation charge reported by Russell et al.,[86] as determined from CV curves similar to those above, as a function of the CO dosing potential. The dramatic difference in CO coverage behavior between Pt and PtRu vs PtMo confirms the very different mechanisms acting in PtMo. The CO coverage decreases with dosing potential for both Pt and PtRu, obviously because of increasing water activation producing OH on the surface to oxidize the CO. This occurs much more dramatically in PtRu because of the ligand mechanism increasing the strength of the Pt−OH bond and lowering the CO oxidation peak for PtRu compared to Pt in the CVs above. However, on PtMo the CO coverage increases with dosing potential. This is exactly as expected when the hydrogen replacement mechanism is dominating, since as the dosing potential is increased, less H_{upd} is present, allowing for more CO to adsorb. Although this data was reported previously, the previously proposed mechanism invoked the Mo (IV/VI) redox couple without further specificity on how this mechanism worked.[18,86]

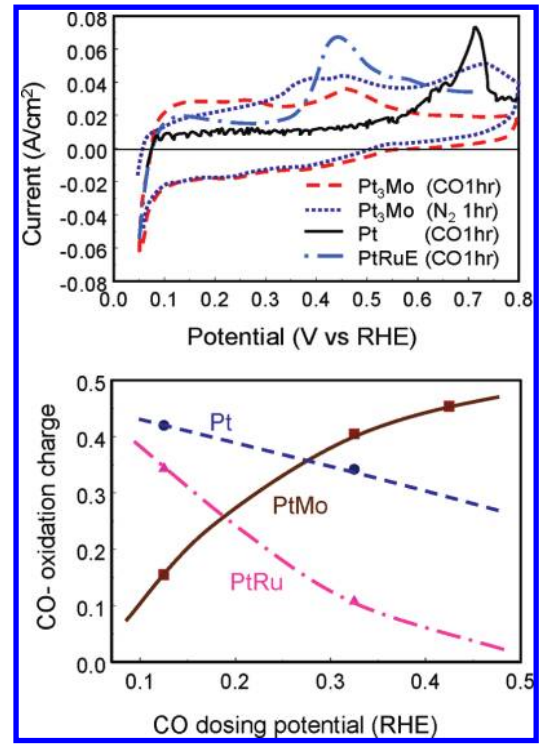

Figure 9. (Top) Cyclic voltammograms obtained in a PEMFC at 55 °C with a 5 cm^2 membrane electrode assembly for the some of the catalysts studied in this work.[18] (Bottom) Charge associated with electro-oxidation of CO species derived from cyclic voltammograms similar to those above for the indicated PtM electrodes from ref 86 after dosing with CO at the potentials indicated. Electrode area 3.14 cm^2, with nearly identical Pt loadings of 0.24 mg(Pt) cm^{-2} geometric for the Pt, PtRu, and PtMo electrodes. Data from ref 86.

We do not suggest that the ligand effect is the same for Sn and oxidized Sn (or Mo and oxidized Mo), only that both Sn and Mo are normally oxidized above 0.2 V when existing as islands on Pt. Other evidence for the importance of the oxidation state of the second metal in PtM bimetallics, and we believe the source of conflicting conclusions on the effect of the second metal is abundant in the literature. For example, consider the PtMo literature first. DFT calculations on a PtMo cluster mimicking the PtMo(111) surface showed very little weakening of the CO−Pt bond, and the reduced barrier to CO oxidation was therefore attributed to a subtle geometric effect of the transition state.[87] On the other hand, similar DFT calculations on a water covered Pt_2Mo(111) surface (i.e., essentially oxidized Mo) showed a drop in the Co−Pt binding energy by a factor of 3 compared to CO/Pt(111) surface.[88] This again reflects the strong dependence on the oxidation state of the Mo. Direct experimental proof for the lower Pt−CO binding in PtMo catalysts was obtained from temperature programmed desorption (TPD) experiments that showed that the linearly adsorbed CO species on a Pt_xMo/TiO_2 sample desorbs at temperatures below 375 K, which is almost 100 K below the CO_L species desorption from Pt/TiO_2.[89] This low desorption temperature of CO/Pt_xMo was attributed to the chemical oxidation at the boundaries of the Mo^{5+} oxide nanoclusters that were detected by XPS as the most abundant oxidation state. Finally recent studies of methanol oxidation over MoOx@Pt core−shell nanoparticles (1−2 ML of Pt over a MoO_x core) revealed incredible CO tolerance, and a threshold for CO oxidation much lower than even traditional PtMo/C catalysts. The authors suggest that a different mechanism other than the bifunctional must be at work in this case and suggest a dramatic weakening of the Pt−CO bond to allow

such a dramatic lowering of the methanol oxidation overpotential.[90] It should be mentioned that the weakened Pt−CO bond for PtMo catalysts is not necessarily the only mechanism for the enhanced CO tolerance, as many papers show a CO reduction peak in the CV curves around 0.4 V, which has been attributed to a bifunctional type mechanism[18,86] but clearly oxidized Mo exhibits a much stronger ligand effect on the Pt−CO binding, and it is probably the dominant role.

Similar apparently conflicting but now understood results have been found for PtSn bimetallic catalysts. For example DFT calculations for $Pt_3Sn(111)$[91,92] show that the Sn has a relative weak effect on the Pt−CO binding, (only 10% reduction[92]). Experimental IR data examining the CO vibrational stretch frequency region also suggest that on $Pt_3Sn(111)$ the CO stretch is only slightly decreased relative to that for CO/Pt(111).[93] Stamenkovic et al. even attribute this small decrease to a coverage effect (i.e., higher) on the $Pt_3Sn(111)$ and therefore appear in this case to not invoke any ligand effect from the Sn on the CO binding to Pt. In these two cases the Sn exists in a reduced state primarily alloyed with the Pt. In contrast, when Sn is added as an adatom on the Pt surface, and therefore existing in an oxidized state, very strong ligand effects have been noted. Nearly 20 years ago, Haner and Ross[44] observed that dissolved Sn species interacting with the surface greatly enhanced methanol oxidation, while PtSn alloys did not. It is well known that SnO_x islands on Pt also dramatically enhance acetaldehyde formation in ethanol oxidation and DFT calculations indicate acetaldehyde formation occurs because of a weakened Pt−C interaction.[94] In work studying the effect of the alloying degree in PtSn/C catalyst on its catalytic behavior for ethanol oxidation, it was found that a PtSn/C catalyst with low alloying degree (i.e., oxidized Sn) enhanced the yield of acetaldehyde products, but a PtSn/C catalyst with high alloying degree (nonoxidized Sn) promoted the overall activity for ethanol oxidation (i.e., enhanced the rate in a different fashion, mostly like CO oxidation via a bifunctional mechanism) but did not decrease the Pt−C bond strength.[95] It seems clear that Mo and Sn show the same varied electronic (ligand) effect on the Pt−C or Pt−CO bond, depending on oxidation state, as Ru, but as will be discussed below, Sn and Mo are mostly oxidized when existing as polyatomic surface islands.

We must carefully distinguish between the ligand effect on the Pt−CO bond and that on the Pt−OH bond (i.e., water activation). The BF and DL CO oxidation mechanisms distinguish the source of the OH involved in eq 3a, i.e., either on the M or near the M island, and the threshold potential for these mechanisms are due to the production of OH via water activation. In Figure 8, no systematic difference with M is found in this threshold, except for the PtRuE catalysts; rather, it shows that the ligand effect is more dependent on particle size. However a significant and systematic trend does appear in the tabulated E_a in Table 3, reflecting the Pt−CO bond strength: $Ru > MoO_x \approx SnO_x > RuO_x$, and this is also reflected in the HR mechanism observed for PtSn and Pt_nMo catalysts. Thus, our results in Figure 8 and previous results in Table 3 are generally consistent; however, this does introduce two puzzling questions:

(1) Why does the ligand effect by these MO_x islands strengthen the Pt−OH bond but weaken the Pt−CO bond?

(2) Why is the HR mechanism not active for the PtRuE catalsyts, if the RuO_x ligand effect is the strongest, as exhibited by the water activation?

The answers to these questions are given in Figures 9 and 10, respectively.

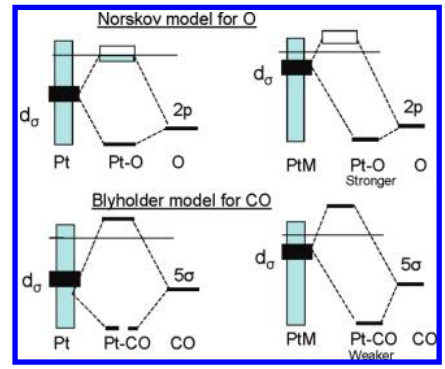

Figure 10. Schematic illustration of the Norskov model for O adsorption and Blyholder model for CO adsorption as discussed in the text.

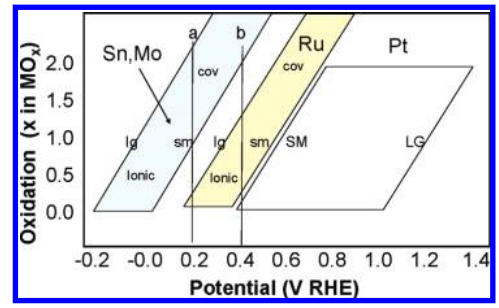

Figure 11. Schematic illustration of Sn, Mo, and Ru island and Pt cluster oxidation levels with potential. The symbols "lg" and "sm" indicate large and small M islands on Pt; LG and SM indicate the size of the Pt clusters. The vertical lines marked a and b denote the potential regions where CO oxidation in reformate and methanol oxidation generally occur, the former assisted by the hydrogen replacement mechanism with PtSn and PtMo, and the latter by the direct ligand mechanism in PtRu.

Figure 9 illustrates the Norskov[96] bonding model for O/Pt and the well-known Blyholder[97] model for CO/Pt. According to the Norskov model for O/Pt, a raising of the Pt d band raises the antibonding Pt−O orbital, which causes charge transfer out of this orbital and hence an increase in the Pt−O bond strength. Thus, first-row transition metals such as Fe, Co, Ni, and Cr, when mixed with Pt generally push down the Pt d band, decrease the Pt−O bond strength, thereby decreasing OH poisoning and increasing the oxidation reaction rate (ORR). In contrast metals such as Mo, Ru, and Sn raise the Pt d band (as shown in Figure 9a), increase the Pt−O bond strength and thereby increase the oxophilicity of the bimetallic cluster and hence water activation. In contrast, a similar raising of the Pt d band makes the Pt−CO band less covalent and weakens the Pt−C bond as illustrated by the Blyholder model,[97] particularly for linearly bonded CO (dominating at higher coverage) when the 5σ orbital dominates the bonding with Pt as discussed above. The Pt−CO antibonding band is sufficiently high that significant charge transfer does not occur for O, and this accounts for the reverse direction in binding with raising of the Pt d band. Indeed even the Pt−O bond can weaken with raising of the d band if the Pt particle is sufficiently small and the Pt−O antibonding band is sufficiently high (the strong coupling limit). Experimental results reported by Koningsberger et al.[98] and DFT results do indeed show this opposite trend for the Pt−OH coverage for small Pt particles. Further evidence for the reversal of the Pt−OH bond strength on small particles is clearly evident from the recent work examining monolayers of PtM on various metals M′ (i.e., ternary systems PtM/M′ with one metal M in the outer monolayer and another M′ as the substrate).[99] In this case the M′ metal reduced the Pt−OH bond strength and coverage by a small amount, and

the M metal by a very large amount. Note the M metal reduced the Pt−OH coverage, not increased it as we find above. Calculations suggest that the MOH−PtOH repulsion was the dominant factor keeping the OH off of the Pt, but a "reverse" electronic ligand effect in the strong coupling limit (single-atom particles) could also be playing a significant role.

Figure 10 provides an answer to question 2 above regarding the absence of the HR mechanism in PtRuE, when the water activation suggests a very strong ligand effect. Mo and Sn are more reactive metals than Pt and oxidize well below 0.2 V, indeed Sn goes to Sn^{2+} already at −0.16 V RHE.[100] In the potential region above 0.0 V, Sn^{2+} even goes to Sn^{4+}, so the Sn islands are always oxidized in the potential region of interest here.[100] The same goes for Mo, indeed Mukerjee and Urian[18] et al. have found that around 0.43−0.50 V, Mo^{4+} goes to Mo^{6+}. However, Figure 10 suggest that an O(H) layer forms in the range of 0.2−0.5 V consistent with CV plots for Ru electrodes, which show oxidation or OH adsorption over the range 0.3 and higher.[101] Thus, Mo and Sn islands are oxidized and exert a strong ligand effect on the Pt throughout the potential range, but Ru is oxidized only above 0.45 V. This explains the lack of the HR mechanism for PtRuE in region a) of the figure, when the RuO_x is already significantly reduced, but a strong ligand effect in region b where the threshold for CO oxidation by adsorbed OH in methanol appears.

This difference between Mo and Ru is revealed very clearly by in situ XAS data reported by Mylswamy et al.[102] on PtMo/C and PtRu/M catalysts. Their Ru K-edge data show oxidiation of the Ru with potential in the range 0.1−1.0 V, with the average oxidation level intermediate between Ru and RuO_2 samples. In contrast, their Mo K-edge data shows the Mo to be mostly oxidized and thus compares more with that for MoO_2. Finally, their whiteline of Pt L_3 edge data shows an increase of intensity with increased M composition. The whiteline intensity increased nearly linearly with Mo atomic fraction but very slow initially with Ru atomic fraction until about 50% Ru when it increased sharply. Assuming this increase results from OH adsorption, it demonstrates again that the electronic ligand effect dramatically increases only when the Ru islands get larger and become oxidized, exactly as expected from the above discussion.

The above emphasizes the importance of the oxidation state of the alloying metal and its effect on Pt. Many studies of Pt on various supports have illustrated the dramatic effect that the acidity of the support can have on the nature of Pt and its reactivity with H, O, and other adsorbates.[103] In general, an acidic (covalent oxide) support causes the bond with H to get weaker and that with O to get stronger (in the strong coupling and small particle limit), and vice versa for basic supports (ionic oxides). Therefore the effect of oxidation of the metal islands in electrocatalysts on Pt has a strong similarity with that established previously in the gas phase where the charge on the O anions of the oxide is the critical parameter.[98,103] By why should RuO_x give a stronger ligand effect than MoO_x and SnO_x at 0.5 V? The electronegativities of the metals (Mo = 1.8, Sn = 2.0, Ru = 2.2[104]) suggest that the full RuO_x oxide should be the least ionic of these three (hence the O anion have the smallest negative charge); however, as illustrated in Figure 10, the RuO_x is only partially oxidized in this potential region and the character of the oxide becomes more covalent with oxidation level (i.e., the oxide ionic character decreases with oxidation level as the metal valence increases). Therefore, the partially oxidized RuO_x (when the oxides is quite ionic) exerts the strongest ligand effect of the three oxides at 0.5 V, but at potentials below 0.2 V this oxide is nearly totally reduced (i.e., RuO_x has returned to OH/Ru or even just Ru when the islands are very small).

Finally, the results reported here easily explain why Pt_nMo is better for HOR in reformate and Pt_nRu for methanol oxidation as exhibited in Table 3. The striking difference in Figure 5a between the CO coverage below 0.3 V for PtSn, PtMo and that for Pt_nRu gives the answer. At low potentials where the HOR occurs, the HR mechanism active with Pt_nMo keeps the catalysts relatively free of CO. However, in methanol, the potential generally rises to 0.3−0.4 V where the strong DL mechanism becomes active, and this mechanism is even better at freeing Pt from CO at this potential. Here it is useful to quote from a paper by Koper,[38] with regard to the different mechanisms at work for CO vs methanol oxidation; "The bifunctional effect is thought to be the dominant mechanism in the catalytic methanol electrooxidation. However, in relation to CO tolerance of the hydrogen oxidation, the current consensus in the electrochemical surface science community seems to shift towards the electronic effect as the dominant mechanism." The results in this work confirm this statement; the electronic weakening of the Pt−CO bond is critical for HOR in reformate, but the bifunctional mechanism, which involves CO oxidation by the OH existing on the second metal or nearby Pt (the latter also as a result of an electronic ligand effect) becomes more important for the MOR.

6. Conclusions

The coverages of CO, H_{upd}, and O(H) on Pt in two different Pt_nMo anodes and a PtSn anode are compared with that previously obtained for three Pt_nRu anodes. The importance of island size and M oxidation state appears to be critical factors in catalyst performance only for PtRu as Sn and Mo islands on the surface (as opposed to Sn and Mo alloyed with Pt) are essentially fully oxidized at all relevant potentials. The ligand effect appears to follow the order Ru < $MoO_n \approx SnO_n$ < RuO_n, with the Pt−OH bond getting stronger and the Pt−CO bond weaker with increasing ligand effect, i.e., oxidation state of the metal M. In retrospect, this should not be surprising, since Ru, a Pt-group metal, shares common properties with Pt, and therefore, an isolated Ru atom shares relatively weak ligand interaction effects with Pt. However, after the formation of larger islands, the metallic-like Ru islands oxidize and have very different properties. Mo and Sn islands on the other hand are very different from Ru, oxidizing at lower potentials and exerting a relatively strong ligand effect at all potentials.

Finally, the data suggest that the catalyst effectiveness in methanol is determined primarily by the bifunctional mechanism enhanced by the MO_x direct ligand effect increasing Pt−OH binding; however, CO tolerance in reformate is determined primarily by the hydrogen replacement mechanism, the latter enhanced by the MO_x ligand effect weakening the Pt−CO binding.

References and Notes

(1) Amphlett, J. C.; Mann, R. F.; Peppley, B. A. *Int. J. Hydrogen Energy* **1996**, *21*, 673.
(2) Kua, J.; Goddard, W. A., III. *J. Am. Chem. Soc.* **1999**, *121*, 10928.
(3) Denis, M. C.; Gouerec, P.; Guay, D.; Dodelet, J. P.; Lalande, G.; Schulz, R. *J. Appl. Electrochem.* **2000**, *30*, 1243.
(4) Tong, Y.; Kim, H. S.; Babu, P. K.; Waszczuk, P.; Wieckowski, A.; Oldfield, E. *J. Am. Chem. Soc.* **2002**, *124*, 468.
(5) Lamouri, A.; Gofer, Y.; Luo, Y.; Chottiner, G. S.; Scherson, D. A. *J. Phys. Chem. B* **2001**, *105*, 6172.

(6) Camara, G. A.; Giz, M. J.; Paganin, V. A.; Ticianelli, E. A. *J. Electroanal. Chem.* **2002**, *537*, 21.
(7) Lin, W. F.; Zei, M. S.; Eiswirth, M.; Ertl, G.; Iwasita, T.; Vielstich, W. *J. Phys. Chem. B* **1999**, *103*, 6968.
(8) Qi, Z.; Kaufman, A. *J. Power Sources* **2003**, *113*, 115.
(9) Viswanathan, R.; Hou, G.; Liu, R.; Bare, S. R.; Modica, F.; Mickelson, G.; Segre, C. U.; Leyarovska, N.; Smotkin, E. S. *J. Phys. Chem. B* **2002**, *106*, 3458.
(10) Lu, C.; Rice, C.; Masel, R. I.; Babu, P. K.; Waszczuk, P.; Kim, H. S.; Oldfield, E.; Wieckowski, A. *J. Phys. Chem. B* **2002**, *106*, 9581.
(11) Koper, M. T. M.; Lebedeva, N. P.; Hermse, C. G. M. *Faraday Discuss.* **2002**, *121*, 301.
(12) Koper, M. T. M.; Lukkien, J. J.; Jansen, A. P. J.; Van Santen, R. A. *J. Phys. Chem. B* **1999**, *103*, 5522.
(13) Koper, M. T. M.; Shubina, T. E.; van Santen, R. A. *J. Phys. Chem. B* **2002**, *106*, 686.
(14) Lebedeva, N. P.; Koper, M. T. M.; Feliu, J. M.; van Santen, R. A. *J. Electroanal. Chem.* **2002**, *524*−*525*, 242.
(15) Lu, C.; Masel, R. I. *J. Phys. Chem. B* **2001**, *105*, 9793.
(16) Watanabe, M.; Motoo, S. *J. Electroanal. Chem. Interfacial Electrochem.* **1975**, *60*, 267. Yajima, T.; Uchida, H.; Watanabe, M. *J. Phys. Chem. B* **2004**, *108*, 2654.
(17) Camara, G. A.; Ticianelli, E. A.; Mukerjee, S.; Lee, S. J.; McBreen, J. *J. Electrochem. Soc.* **2002**, *149*, A748.
(18) Mukerjee, S.; Urian, R. C. *Electrochim. Acta* **2002**, *47*, 3219.
(19) Urian, R. C.; Gulla, A. F.; Mukerjee, S. *J. Electroanal. Chem.* **2003**, *554*−*555*, 307.
(20) Lee, S. J.; Mukerjee, S.; Ticianelli, E. A.; McBreen, J. *Electrochim. Acta* **1999**, *44*, 3283.
(21) Mukerjee, S.; Urian, R. C.; Lee, S. J.; Ticianelli, E. A.; McBreen, J. *J. Electrochem. Soc.* **2004**, *151*, A1094.
(22) Russell, A. E.; Maniguet, S.; Mathew, R. J.; Yao, J.; Roberts, M. A.; Thompsett, D. *J. Power Sources* **2001**, *96*, 226.
(23) Waszczuk, P.; Wieckowski, A.; Zelenay, P.; Gottesfeld, S.; Coutanceau, C.; Leger, J. M.; Lamy, C. *J. Electroanal. Chem.* **2001**, *511*, 55.
(24) Lu, G. Q.; White, J. O.; Wieckowski, A. *Surf. Sci.* **2004**, *564*, 131.
(25) Lu, G. Q.; Waszczuk, P.; Wieckowski, A. *J. Electroanal. Chem.* **2002**, *532*, 49.
(26) Brankovic, S. R.; Marinkovic, N. S.; Wang, J. X.; Adzic, R. R. *J. Electroanal. Chem.* **2002**, *532*, 57.
(27) Kuk, S. T.; Wieckowski, A. *J. Power Sources* **2005**, *141*, 1.
(28) Spendelow, J. S.; Lu, G. Q.; Kenis, P. J. A.; Wieckowski, A. *J. Electroanal. Chem.* **2004**, *568*, 215.
(29) Lin, W. F.; Iwasita, T.; Vielstich, W. *J. Phys. Chem. B* **1999**, *103*, 3250.
(30) McGovern, M. S.; Waszczuk, P.; Wieckowski, A. *Electrochim. Acta* **2006**, *51*, 1194.
(31) Gasteiger, H. A.; Markovic, N.; Ross, P. N., Jr.; Cairns, E. J. *J. Phys. Chem.* **1994**, *98*, 617.
(32) Massong, H.; Wang, H.; Samjeske, G.; Baltruschat, H. *Electrochim. Acta* **2000**, *46*, 701.
(33) Grgur, B. N.; Markovic, N. M.; Ross, P. N., Jr. *J. Phys. Chem. B* **1998**, *102*, 2494.
(34) Grgur, B. N.; Markovic, N. M.; Ross, P. N. *J. Electrochem. Soc.* **1999**, *146*, 1613.
(35) Grgur, B. N.; Zhuang, G.; Markovic, N. M.; Ross, P. N., Jr. *J. Phys. Chem. B* **1997**, *101*, 3910.
(36) McBreen, J.; Mukerjee, S. *J. Electrochem. Soc.* **1995**, *142*, 3399.
(37) Mukerjee, S.; McBreen, J. *J. Electrochem. Soc.* **1999**, *146*, 600.
(38) Koper, M. T. M. *Surf. Sci.* **2004**, *548*, 1.
(39) Gallagher, M. E.; Lucas, C. A.; Stamenkovic, V.; Markovic, N. M.; Ross, P. N. *Surf. Sci.* **2003**, *544*, L729.
(40) Morimoto, Y.; Yeager, E. B. *J. Electroanal. Chem.* **1998**, *444*, 95.
(41) Wang, K.; Gasteiger, H. A.; Markovic, N. M.; Ross, P. N., Jr. *Electrochim. Acta* **1996**, *41*, 2587.
(42) Gasteiger, H. A.; Markovic, N. M.; Ross, P. N., Jr. *J. Phys. Chem.* **1995**, *99*, 8945.
(43) Paffett, M. T.; Gebhard, S. C.; Windham, R. G.; Koel, B. E. *J. Phys. Chem.* **1990**, *94*, 6831.
(44) Haner, A. N.; Ross, P. N. *J. Phys. Chem.* **1991**, *95*, 3740.
(45) Markovic, N. M.; Widelov, A.; Ross, P. N.; Monteiro, O. R.; Brown, I. G. *Catal. Lett.* **1997**, *43*, 161.
(46) Xiao, X.-Y.; Tillmann, S.; Baltruschat, H. *Phys. Chem. Chem. Phys.* **2002**, *4*, 4044.
(47) Stamenkovic, V. R.; Arenz, M.; Lucas, C. A.; Gallagher, M. E.; Ross, P. N.; Markovic, N. M. *J. Am. Chem. Soc.* **2003**, *125*, 2736.
(48) Hayden, B. E.; Rendall, M. E.; South, O. *J. Am. Chem. Soc.* **2003**, *125*, 7738.
(49) Arenz, M.; Stamenkovic, V.; Ross, P. N.; Markovic, N. M. *Electrochem. Commun.* **2003**, *5*, 809.
(50) Goetz, M.; Wendt, H. *J. Appl. Electrochem.* **2001**, *31*, 811.
(51) Skelton, D. C.; Tobin, R. G.; Lambert, D. K.; DiMaggio, C. L.; Fisher, G. B. *J. Phys. Chem. B* **1999**, *103*, 964.
(52) Brankovic, S. R.; Wang, J. X.; Adzic, R. R. *Electrochem. Solid-State Lett.* **2001**, *4*, A217.
(53) Scott, F. J.; Mukerjee, S.; Ramaker, D. E. *J. Electrochem. Soc.* **2007**, *154*, A396.
(54) Watanabe, M.; Uchida, M.; Motoo, S. *J. Electroanal. Chem. Interfac. Electrochem.* **1987**, *229*, 395.
(55) Mukerjee, S.; Srinivasan, S.; Soriaga, M. P. *J. Electrochem. Soc.* **1995**, *142*, 1409.
(56) Urian, R. C. Ph.D. Dissertation, Northeastern University, (2002).
(57) Teliska, M.; O'Grady, W. E.; Ramaker, D. E. *J. Phys. Chem. B* **2004**, *108*, 2333. 2005, *109*, 8076.
(58) Koningsberger, D. E.; de Graaf, J.; Mojet, B. L.; Ramaker, D. E.; Miller, J. T. *Appl. Catal., A* **2000**, *191*, 205.
(59) Mojet, B. L.; Miller, J. T.; Ramaker, D. E.; Koningsberger, D. C. *J. Catal.* **1999**, *186*, 373.
(60) Ramaker, D. E.; Mojet, B. L.; Garriga Oostenbrink, M. T.; Miller, J. T.; Koningsberger, D. C. *Phys. Chem. Chem. Phys.* **1999**, *1*, 2293.
(61) Koningsberger, D. C.; Oudenhuijzen, M. K.; Bitter, J. H.; Ramaker, D. E. *Top. Catal.* **2000**, *10*, 167.
(62) Mojet, B. L.; Ramaker, D. E.; Miller, J. T.; Koningsberger, D. C. *Catal. Lett.* **1999**, *62*, 15.
(63) Ramaker, D. E.; Koningsberger, D. C. *Phys. Rev. Lett.* **2002**, *89*, 139701.
(64) Teliska, M.; Murthi, V. S.; Mukerjee, S.; Ramaker, D. E. *J. Electrochem. Soc.* **2005**, *152*, A2159.
(65) Roth, C.; Benker, N.; Buhrmester, T.; Mazurek, M.; Loster, M.; Fuess, H.; Koningsberger, D. C.; Ramaker, D. E. *J. Am. Chem. Soc.* **2005**, *127*, 14607.
(66) Ravel, B.; Newville, M. *J. Synch. Rad.* **2005**, *12*, 537.
(67) Newville, M.; Livins, P.; Yacoby, Y.; Rehr, J. J.; Stern, E. A. *Phys. Rev. B: Condens. Matter Mater. Phys.* **1993**, *47*, 14126.
(68) Scott, F. J.; Roth, C.; Ramaker, D. E. *J. Phys. Chem. C* **2007**, *111*, 11403.
(69) Zabinsky, S. I.; Rehr, J. J.; Aukudinov, A.; Albers, R. C.; Eller, M. J. *Phys. Rev. B: Condens. Matter* **1995**, *52*, 2995.
(70) Janin, E.; von Schenck, H.; Gothelid, M.; Karlsson, U. O.; Svensson, M. *Phys. Rev. B: Condens. Matter Mater. Phys.* **2000**, *61*, 13144.
(71) de Graaf, J.; J.van Dillen, A.; de Jong, K. P.; Koningsberger, D. C. *J. Catal.* **2001**, *203*, 307.
(72) Ramaker, D. E.; Oudenhuijzen, M. K.; Koningsberger, D. C. *J. Phys. Chem. B* **2005**, *109*, 5608.
(73) H = 6.9, CO = 3.3, OH = 4.0, and O = 1.7.
(74) Ji, Y.; Koot, V.; van der Eerden, A. M. J.; Weckhuysen, B. M.; Koningsberger, D. C.; Ramaker, D. E. *J. Catal.* **2007**, *245*, 413.
(75) Villegas, I.; Weaver, M. J. *J. Chem. Phys.* **1994**, *101*, 1648.
(76) Wang, J. X.; Markovic, N. M.; Adzic, R. R. *J. Phys. Chem. B* **2004**, *108*, 4127.
(77) Xu, H.; Brosha, E. L.; Garzon, F. H.; Uribe, F.; Wilson, M.; Pivovar, B. *E.C.S. Trans.* **2007**, *11*, 282.
(78) Chlistunoff, J.; Uribe, F.; Pivovar, B. *E.C.S.Trans.* **2006**, *1*, 137.
(79) Aleksandrova, E.; Hiesgen, R.; Eberhard, D.; Friedrich, K. A.; Kaz, T.; Roduner, E. *Chem. Phys. Chem.* **2007**, *8*, 519.
(80) Gasteiger, H. A.; Kocha, S. S.; Sompalli, B.; Wagner, F. T. *Appl. Catal. B: Environ.* **2005**, *56*, 9.
(81) Shinozaki, H. K.; Hatanaka, T.; Morimoto, Y. *E.C.S. Trans.* **2007**, *11*, 497.
(82) Gatewood, D.; Ramaker, D. E.; Swider-Lyons, K. E. unpublished.
(83) Rossmeisl, J.; Norksov, J. K.; Taylor, C. D.; Janik, M. J.; Neurock, M. *J. Phys. Chem. B* 218332006.
(84) Baldelli, S.; Markovic, N.; Ross, P.; Shen, Y.-R.; Somorjai, G. *J. Phys. Chem. B* **1999**, *103*, 8920.
(85) Mojet, B. L.; Miller, J. T.; Koningsberger, D. C. *J. Phys. Chem. B* **1999**, *103*, 2724.
(86) Russell, A. E.; Ball, S. C.; Maniguet, S.; Thompsett, D. *J. Power Sources* **2007**, *171*, 72.
(87) Ji, Z.; Li, J.-Q. *Chem. Phys. Lett.* **2006**, *424*, 111. Li, Z.; Jalbout, A. F.; Li, J.-Q. *Solid State Commun.* **2007**, *142*, 148.
(88) Wang, J. G.; Hammer, B. *J. Catal.* **2006**, *243*, 192.
(89) Zafeiratos, S.; Papakonstantinou, G.; Jacksic, M. M.; Neophytides, S. G. *J. Catal.* **2005**, *232*, 127.
(90) Liu, Z.; Hu, J. E.; Wang, Q.; Gaskell, K.; Frenkel, A. I.; Jackson, G. S.; Eichhorn, B. *J. Am. Chem. Soc.* **2009**, *131*, 6924.
(91) Sümer, A.; Aksoylu, A. E. *Surf. Sci.* **2008**, *602*, 1636.
(92) Dupont, C.; Jugnet, Y.; Loffreda, D. *J. Am. Chem. Soc.* **2006**, *128*, 9129.
(93) Stamenkovic, V.; Arenz, M.; Blizanac, B. B.; Mayrhofer, K. J. J.; Ross, P. N.; Markovic, N. M. *Surf. Sci.* **2005**, *576*, 145–157.
(94) Wang, H.-F.; Liu, Z.-P. *J. Am. Chem. Soc.* **2008**, *130*, 10996.
(95) Zhua, M.; Suna, G.; Xina, Q. *Electrochim. Acta* **2009**, *54*, 1511.

(96) Hammer, B.; Nørskov, J. K. *Nature* **1995**, *376*, 238. Stamenkovic, V.; Moon, B. S.; Mayrhofer, J. J.; Ross, P. N.; Markovic, N. M.; Rossmeisl, J.; Greeley, J.; Nørskov, J. K. *Angew. Chem., Int. Ed.* **2006**, *18*, 2815.

(97) Blyholder, G. J. *J. Phys. Chem.* **1975**, *79*, 756.

(98) Ramaker, D. E.; Teliska, M.; Zhang, Y.; Stakheev, A. Yu.; Koningsberger, D. C. *Phys. Chem. Chem. Phys.* **2003**, *5*, 4492.

(99) Nilekar, A. U.; Xu, Y.; Zhang, J.; Vukmirovic, M. B.; Sasaki, K.; Adzic, R. R.; Mavrikakis, M. *Top Catal* **2007**, *46*, 276.

(100) Gatewood, D.; Ramaker, D. E.; Swider-Lyons, K. E. *J. Electrochem. Soc.* **2008**, *155*, B834.

(101) Cao, D.; Wieckowski, A.; Inukai, J.; Alonso-Vante, N. *J. Electrochem. Soc.* **2006**, *153*, A869.

(102) Mylswamy, S.; Wang, C. Y.; Liu, R. S.; Lee, J.-F.; Tang, M.-J.; Lee, J.-J.; Weng, B.-J. *Chem. Phys. Lett.* **2005**, *412*, 444.

(103) Oudenhuijzen, M. K.; van Bokhoeven, J. A.; Ramaker, D. E.; Koningsberger, D. C. *J. Phys. Chem. B* **2004**, *108*, 20247.

(104) Atkins, P. W. *Physical Chemistry*, 3rd ed.; W. H. Freeman and Co.: New York, 1986; p 823.

JP908582R